AIP | Journal of Applied Physics

Analysis of the series resistance in pin-type thin-film silicon solar cells

Thomas C. M. Müller, Bart E. Pieters, Uwe Rau, and Thomas Kirchartz

Citation: Journal of Applied Physics **113**, 134503 (2013); doi: 10.1063/1.4798393
View online: http://dx.doi.org/10.1063/1.4798393
View Table of Contents: http://scitation.aip.org/content/aip/journal/jap/113/13?ver=pdfcov
Published by the AIP Publishing

Analysis of the series resistance in *pin*-type thin-film silicon solar cells

Thomas C. M. Müller,[1,a)] Bart E. Pieters,[1] Uwe Rau,[1] and Thomas Kirchartz[2]
[1]*IEK5–Photovoltaik, Forschungszentrum Jülich, 52425 Jülich, Germany*
[2]*Department of Physics, Imperial College London, South Kensington SW7 2AZ, United Kingdom*

(Received 27 January 2013; accepted 13 March 2013; published online 1 April 2013)

The series resistance of microcrystalline hydrogenated silicon thin-film *pin*-type solar cells is investigated using illumination dependent current/voltage characteristics. We present a simple analytical model describing the total series resistance of low-mobility *pin*-type solar cells. The model thus provides insight into the influence of the material properties of the intrinsic layer on the series resistance. Our model allows us to separate the voltage dependent internal resistance of the intrinsic layer from the residual, external resistance. We verified our model over a wide range of parameters relevant to thin-film silicon devices by comparison to numerical simulations. Finally, we demonstrate that our model can consistently describe the series resistance of experimental a μc-Si:H *pin*-type solar cell. Furthermore, the fitting of the model with experimental data yields the external series resistance and information of the carrier mobilities and effective density of states in the bands of the intrinsic layer in the device. © *2013 American Institute of Physics*. [http://dx.doi.org/10.1063/1.4798393]

I. INTRODUCTION

Series resistance in solar cells is unavoidable and often relevant to the achieved efficiency.[1–4] Moreover, advanced characterization techniques like electroluminescence imaging,[5–11] or lock-in thermography[12,13] in solar cells are often affected by the series resistance. In this work, we analyze the series resistance in hydrogenated amorphous (a-Si:H) or hydrogenated microcrystalline (μc-Si:H) silicon solar cells. The series resistance of these devices is not only affected by the contacting scheme. Also material properties of the silicon layers and the *pin*-type device structure have a profound affect on the series resistance.

The present paper uses the classical method of Wolf and Rauschenbach[14] to determine the series resistance (R_s) by comparison of dark and illuminated current/voltage (JV) characteristics. This method, usually denoted as J_{sc}/V_{oc}-method, is especially useful in situations where R_s is dependent on bias voltage and/or illumination level.

To analyze the determined series resistance we developed a simple analytical model. This model distinguishes between internal and external series resistance. We define the internal series resistance as the series resistance that originates within the silicon layer stack and the external series resistance as the series resistance arising form, the contacting scheme. Our analytical model describes the internal series resistance with only a few material parameters and thus is useful in understanding series resistance effects and can aid in determining material properties of the intrinsic layer within a solar cell.

We compare our analytical model for the internal series resistance to numerical simulations using the program *Advanced Semiconductor Analysis* (ASA).[15] Furthermore, we experimentally determined the series resistance of μc-Si:H thin-film solar cells as a function of voltage and temperature. We demonstrate that our analytical model consistently describes the observed series resistances.

a)E-mail: t.c.m.mueller@fz-juelich.de.

In Sec. II, we introduce the principle of the series J_{sc}/V_{oc}-method for determining the series resistance. The analytical model for the internal series resistance is introduced in Sec. III. In Sec. IV, we compare the analytical model with simulation results and experimentally determined series resistances of a μc-Si:H solar cell.

II. THE J_{sc}/V_{oc} METHOD FOR DETERMINATION OF SERIES RESISTANCE

The analysis of the series resistance via the J_{sc}/V_{oc}-method relies on the superposition of the dark current density (J_d) and the photocurrent (J_{ph}) and their dependence on the voltage (V) applied to the device such that the total current reads

$$J = J_d(V - JR_s) - J_{ph}, \tag{1}$$

where the internal junction voltage (V_j) depends on the external voltage (V) via

$$V_j = V - JR_s. \tag{2}$$

Under open circuit conditions, we have $J = 0$ and, therefore,

$$J_{ph} = J_d(V) = J_d(V_{oc}). \tag{3}$$

If (and only if) the photocurrent (J_{ph}) is independent from V, we can identify J_{ph} with the short circuit current density (J_{sc}).

Finally, the J_{sc}/V_{oc}-method uses a series of J_{sc}/V_{oc} pairs under various illumination intensities (ϕ) and compares each pair with the JV-curve measured in the dark at equal current densities,

$$J_d(V - J_dR_s) = J_{sc}(\phi) = J_{sc}(V_{oc}). \tag{4}$$

Because of the equality of current densities, the voltage arguments on the left and on the right side in Eq. (4) must be equal such that

$$V - J_d R_s = V_{oc}. \tag{5}$$

Finally, resolving Eq. (5) for R_s yields

$$R_s = (V - V_{oc})/J_d. \tag{6}$$

The Fig. 1 illustrates, how we use Eq. (6) to determine R_s at a given dark current (J_d).

In the following, we use Eq. (6) as a definition of the series resistance (R_s) resulting from the J_{sc}/V_{oc}-method regardless whether or not the actual device follows the superposition principle. The physical interpretation of experimentally obtained R_s values might therefore cover much more than a simple Ohmic resistance.[14] For a *pin* device, we differentiate between an internal, voltage dependent resistance of the junction ($R_s^i(V)$), and an external, constant series resistance (R_s^e). This yields

$$R_s(V) = R_s^e + R_s^i(V). \tag{7}$$

III. ANALYTICAL APPROXIMATION FOR THE *i*-LAYER RESISTANCE

For the calculation of the internal series resistance (R_s^i) of a *pin*-device, we assume flat quasi-Fermi level splitting over the depth of the intrinsic layer (w), which is equal to the junction voltage (V) at the contacts. The Fig. 2 illustrates $qV = E_{fn} - E_{fp}$ for the quasi Fermi-levels (E_{fn}, E_{fp}) of the conduction and valence band, respectively, where q is the elementary charge. To describe the electric field (F_0) in the center region of the intrinsic layer, we use a *built-in* voltage (V_{bi}) caused by the doped layers. A scaling factor γ takes the band bending at the *p-i* and *i-n* interfaces into account. Furthermore, we assume a homogeneous electric field (F_0) in the center region of the intrinsic layer,

$$F_0 = \gamma \frac{V_{bi} - V}{w}. \tag{8}$$

Using device simulations, we find this scaling factor (γ) in *pin*-type thin-film silicon solar cells typically in the range $0.25 \leq \gamma \leq 0.45$.

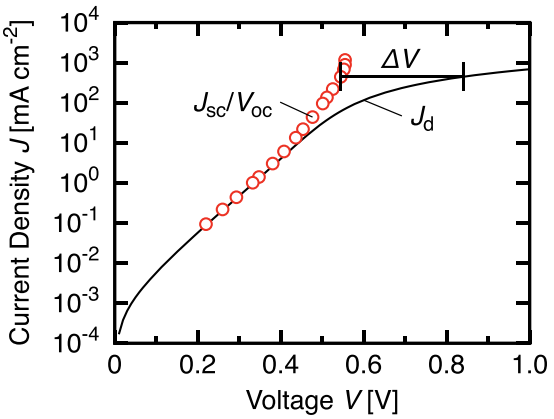

FIG. 1. Determination of series resistance (R_s) from the difference (ΔV) of the voltage in the dark (V_d) and the voltage (V_{oc}) under different illumination intensities at a given current density $J = J_{sc}$ corresponding to V_{oc}. A dark J/V characteristic (black solid line) and pairs of J_{sc} and V_{oc} (red open circles) are shown.

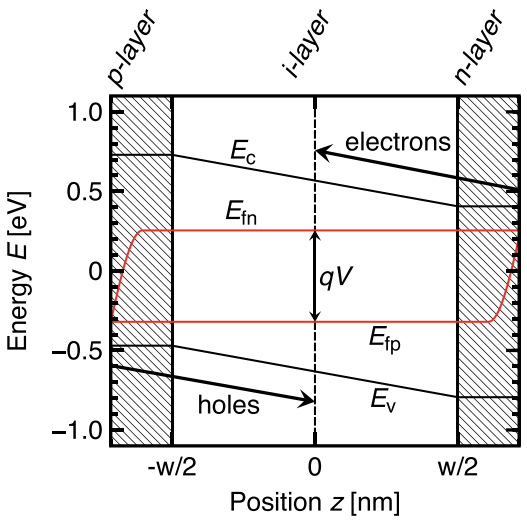

FIG. 2. Schematic band-diagram of a μc-Si:H *pin*-type solar cell with an intrinsic absorber layer of thickness w under illumination. The energy positions of the conduction band, valence band, and the electron/hole quasi Fermi-levels are denoted as E_c, E_v, E_{fn}, and E_{fp}, respectively.

The conductivity of the valence and conduction band is $\sigma_h = qp\mu_h$ and $\sigma_e = qn\mu_e$, respectively, where μ_h and μ_e are the band mobilities for holes and electrons. The charge carrier concentrations for holes and electrons are given by p and n.

In the dark, most recombination takes place, where the charge carrier concentrations are approximately the same, i.e., $n \approx p$. This is placed in the middle of the intrinsic layer at $z = 0$.[15] We simplify this recombination profile by assuming all recombination takes place exactly in the middle (see Fig. 2). Thus, the internal series resistance,

$$R_s^i = R_e + R_h, \tag{9}$$

can be written as the sum of two terms taking into account the transport of electrons in the half of the device closer to the electron contact (R_e) and holes in the half closer to the hole contact (R_h). The contributions for electrons and holes follow from integrating over the inverse conductivity as

$$R_e = \int_0^{w/2} \frac{1}{q\mu_e n(z)} dz \tag{10a}$$

for electrons and

$$R_h = \int_{-w/2}^{0} \frac{1}{q\mu_h p(z)} dz \tag{10b}$$

for holes.

Therefore, the charge carrier concentrations read

$$n = N(T) \exp\left(\frac{E_{fn} - E_c}{kT}\right) \tag{11a}$$

and

$$p = N(T) \exp\left(\frac{E_v - E_{fp}}{kT}\right), \tag{11b}$$

where the temperature dependence of the effective density of states given by $N(T) = N_{T_0}(T/T_0)^{3/2}$ is related to a corresponding reference temperature (T_0).[16] We assume the effective densities of states at conduction and valence band edge to be the same, i.e., $N_{c,T_0} = N_{v,T_0} = N_{T_0}$.

The intrinsic charge carrier concentration (n_0) in the middle of the *i*-layer can be derived by symmetrizing the electron and hole concentration from Eq. (11) with $n_0^2 = np$. This leads together with

$$n(z) = n_0 \exp\left(\frac{qF_0}{kT} z\right) \tag{12a}$$

and

$$p(z) = n_0 \exp\left(-\frac{qF_0}{kT} z\right), \tag{12b}$$

and $E_c - E_v = E_\mu$ for the mobility gap between conduction (E_c) and valence band edge (E_v) to

$$n_0(T) = N_{T_0}\left(\frac{T}{T_0}\right)^{3/2} \exp\left(\frac{qV - E_\mu}{2kT}\right). \tag{13}$$

Substituting Eqs. (8), (12), and (13) in Eq. (10) yields

$$\begin{aligned} R_e(V, T) = {} & \frac{1}{\mu_e}\frac{1}{qN_{T_0}}\left(\frac{T}{T_0}\right)^{-3/2} \exp\left(\frac{E_\mu - qV}{2kT}\right) \\ & \times \frac{kT\,w}{\gamma\, q(V - V_{bi})} \\ & \times \exp\left[\frac{\gamma\, q(V - V_{bi})}{kT\,w} z\right]_0^{w/2} \end{aligned} \tag{14a}$$

and analog

$$\begin{aligned} R_h(V, T) = {} & \frac{1}{\mu_h}\frac{1}{qN_{T_0}}\left(\frac{T}{T_0}\right)^{-3/2} \exp\left(\frac{E_\mu - qV}{2kT}\right) \\ & \times \left(-\frac{kT\,w}{\gamma\, q(V - V_{bi})}\right) \\ & \times \exp\left[-\frac{\gamma\, q(V - V_{bi})}{kT\,w} z\right]_{-w/2}^{0}. \end{aligned} \tag{14b}$$

Combining the Eqs. (14a) and (14b) with Eqs. (7) and (9) leads to

$$\begin{aligned} R_s(V, T) = {} & R_s^e + \frac{1}{qN_{T_0}}\left(\frac{T_0}{T}\right)^{3/2} \exp\left(\frac{E_\mu - qV}{2kT}\right) \\ & \times \left(\frac{1}{\mu_h} + \frac{1}{\mu_e}\right) \frac{kT\,w}{\gamma\, q(V - V_{bi})} \\ & \times \left[\exp\left(\frac{\gamma\, q(V - V_{bi})}{2kT}\right) - 1\right]. \end{aligned} \tag{15}$$

Note that $qN_{T0}\mu_e$ and $qN_{T0}\mu_h$ are the minimum metallic conductivities of the conduction and valence band, respectively.[17] Thus the term $qN_{T0}\,(1/\mu_h + 1/\mu_e)^{-1}$ in this Eq. (15) constitutes the parallel minimum metallic conductivity of the conduction and valence band. The mobilities in Eq. (15) are band mobilities (i.e., unaffected by trapping processes) and not drift mobilities as, e.g., determined from *time-of-flight* measurements.[18–24]

We simplify Eq. (15) for $V < V_{bi}$ and obtain

$$R_s(V, T) = R_s^e + w\,\rho_{s,0}^i(T) \exp\left(-\frac{qV}{2kT}\right), \tag{16}$$

where $\rho_{s,0}^i(T)$ is determined by the material properties of the intrinsic layer and the built in potential in the device. The exponential term in Eq. (16) dominates the voltage dependency of the internal series resistance and arises from the voltage dependency of the charge carrier concentrations in the device.

It is also important to note that in the present derivation, we assume that the quasi-Fermi levels are constant through the device, i.e., $\nabla E_{fn} = \mathbf{0}$. Although this assumption is usually reasonable, it actually neglects the effects of R_s^i, which results in a gradient in quasi-Fermi levels $\mathbf{J} = qn\mu_e \nabla E_{fn}$. Consequently, it is important to analyze the influence of the simplifications by comparison between our simple model and numerical device simulations, as will be presented in the following.

IV. RESULTS

A. Simulation

To test the accuracy of Eq. (15), we perform one-dimensional simulations using the numerical device simulator ASA.[25–28] The optical modeling uses the multi rough-interface model, which is part of ASA.[29,30] The parameters, which are used here, are based on[15] for μc-Si:H, and[22,31,32] for a-Si:H. The parameters are shown in Table I for the intrinsic layers of a μc-Si:H and a-Si:H *pin*-type solar cell, where ε_r is the dielectric constant, $E_{v,c0}$ the characteristic energy, and $N_{v,c0}$ the effective density of states of the valence and conduction band tail, respectively. The correlation energy of the dangling bonds is given by U, and the total dangling bond concentration by N_{db}. The $\sigma_{e,h}$ are the capture cross-sections for electrons and holes each.

The series resistance is finally calculated from the simulated *JV* characteristics using Eq. (6) in the same way as for experimental data in Subsection IV B.

In a first step, we model the influence of the *built-in* voltage (V_{bi}) on the numerical value of R_s. The Fig. 3 compares these results for a μc-Si:H *pin*-type solar cell. The V_{bi} in the numerical simulations is tuned by the choice of the activation energies (E_{ap}, E_{an}) of the *p*- and *n*-doped layer, respectively. The *built-in* voltage is calculated from

$$V_{bi} = \chi_p - \chi_n + E_{\mu p} - E_{ap} - E_{an}, \tag{17}$$

where for μc-Si:H $\chi_p - \chi_n = 0.15\,\text{eV}$ is the difference between the electron affinities of the *p*- and *n*-doped layer, respectively.[15] The used activation energies for each of the four simulated *built-in* potentials in Fig. 3 are ($E_{ap} = 0.10$, 0.15, 0.20, 0.25 eV, and $E_{an} = 0.25$, 0.30, 0.35, 0.40 eV) for the *p*- and *n*-doped layer, respectively.

The Fig. 3 shows for μc-Si:H *pin*-type solar cells that the *built-in* voltage in a range $0.75\,\text{V} \le V_{bi} \le 1.05\,\text{V}$ has only a small influence on the simulated series resistance as well as on

TABLE I. Parameters of intrinsic layer for numerical simulations at a temperature $T_0 = 300\,\mathrm{K}$ of μc-Si:H,[15] and a-Si:H[22,31,32] *pin*-type solar cells.

	μc-Si:H	a-Si:H	Unit
	Structure		
d	1150	330	nm
	Transport, doping, and delocalized states		
E_μ	1.18	1.75	eV
ε_r	11.9	11.9	—
X	4.05	4.00	eV
N_v	2×10^{19}	2×10^{20}	cm^{-3}
N_c	2×10^{19}	2×10^{20}	cm^{-3}
μ_e	37	10	$\mathrm{cm}^2\,\mathrm{V}^{-1}\,\mathrm{s}^{-1}$
μ_h	12	4	$\mathrm{cm}^2\,\mathrm{V}^{-1}\,\mathrm{s}^{-1}$
	Valence-band tails		
E_{v0}	31	43	meV
N_{v0}/N_v	30	15	eV^{-1}
σ_h^0	3.0×10^{-16}	0.7×10^{-16}	cm^2
σ_e^+	30×10^{-16}	7.0×10^{-16}	cm^2
	Conduction-band tails		
E_{c0}	31	30	meV
N_{c0}/N_c	30	25	eV^{-1}
σ_e^0	3.0×10^{-16}	0.7×10^{-16}	cm^2
σ_h^-	30×10^{-16}	7.0×10^{-16}	cm^2
	Dangling bonds		
U	0.2	0.2	eV
N_{db}	7.5×10^{15}	1.6×10^{16}	cm^{-3}
σ_h^0	3.0×10^{-16}	1.0×10^{-16}	cm^2
σ_e^0	3.0×10^{-16}	1.0×10^{-16}	cm^2
σ_h^-	30×10^{-16}	10×10^{-16}	cm^2
σ_e^+	30×10^{-16}	10×10^{-16}	cm^2
	Electronic contact		
R_s^e	0.4	0.4	$\Omega\,\mathrm{cm}^2$

the analytical approach given by Eq. (15). This analytical expression Eq. (15) slightly overestimates the influence of V_{bi}, but the influence of the relatively large variation of V_{bi} is still small. In the following, we use $V_{bi}(E_{ap} = 0.15\,\mathrm{eV}, E_{an} = 0.30\,\mathrm{eV}) = 0.95\,\mathrm{V}$ and $\gamma = 0.30$ for μc-Si:H, and $V_{bi}(E_{ap} = 0.45\,\mathrm{eV}, E_{an} = 0.25\,\mathrm{eV}) = 1.15\,\mathrm{V}$ and $\gamma = 0.25$ for a-Si:H.

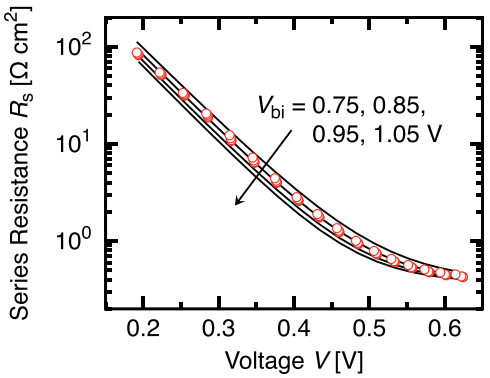

FIG. 3. Dependence of series resistance (R_s) of a μc-Si:H *pin*-type solar cell on *built-in* voltage $V_{bi} = 0.75, 0.85, 0.95, 1.05\,\mathrm{V}$ as derived from Eq. (15) (black solid lines) and derived from numerical simulations (red open circles).

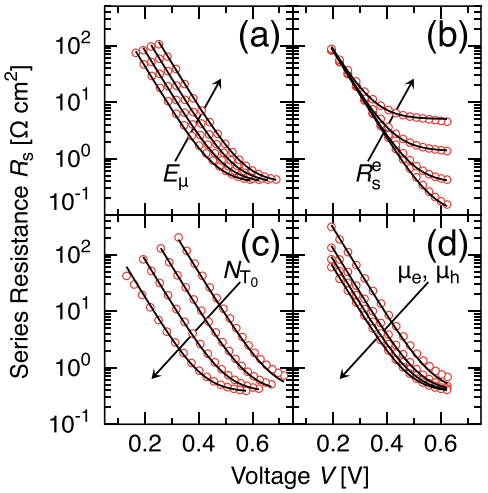

FIG. 4. Comparison between the results of numerical simulations (red open circles) and the analytical approximation from Eq. (15) (black solid lines) for a μc-Si:H *pin*-type solar cell. In every subfigure, one parameter is varied: (a) mobility gap energy $E_\mu = 1.15, 1.18, 1.22, 1.25\,\mathrm{eV}$, (b) external series resistance $R_s^e = 0.1, 0.4, 1.4, 5.0\,\Omega\,\mathrm{cm}^2$, (c) effective densities of states $N_{T0} = 1 \times 10^{18}, 5 \times 10^{18}, 2 \times 10^{19}, 1 \times 10^{20}\,\mathrm{cm}^{-3}$, and (d) charge carrier mobilities for electrons $\mu_e = 10, 23, 37, 50\,\mathrm{cm}^2\,\mathrm{V}^{-1}\,\mathrm{s}^{-1}$ and holes $\mu_h = 1/3\,\mu_e$. As baseline parameters serve the following values: $E_\mu = 1.18\,\mathrm{eV}$, $R_s^e = 0.4\,\Omega\,\mathrm{cm}^2$, $N_{T0} = 2 \times 10^{19}\,\mathrm{cm}^{-3}$, and $\mu_e = 37\,\mathrm{cm}^2\,\mathrm{V}^{-1}\,\mathrm{s}^{-1}$.

In a next step, we vary the parameters E_μ, R_s^e, N_{T_0}, as well as μ_e and μ_h (fixed ratio $\mu_e = 3\,\mu_h$) and compare the ASA simulations with Eq. (15). The results are shown in Fig. 4 for a μc-Si:H *pin*-solar cell and in Fig. 5 for an a-Si:H device. For the variation of a single parameter, we use a reference set of parameters shown in Table I as a starting point. Only one parameter is changed and the effect on R_s is shown in its corresponding subfigure. It can be seen that Eq. (15) fits very well to the numerical simulations over broad spectra

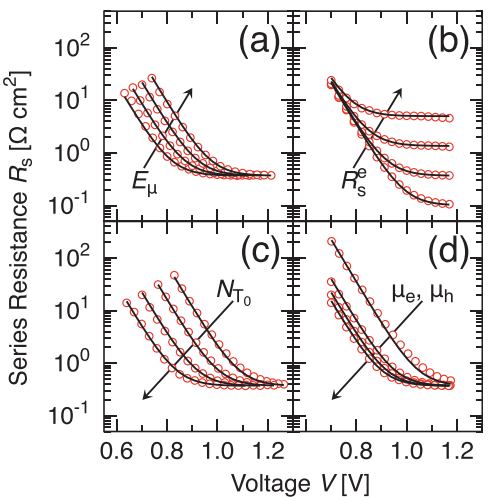

FIG. 5. Comparison between the results of numerical simulations (red open circles) and the analytical approximation from Eq. (15) (black solid lines) for a-Si:H *pin*-type solar cell. In every subfigure, one parameter was varied: (a) mobility gap energy $E_\mu = 1.65, 1.70, 1.75, 1.80\,\mathrm{eV}$, (b) external series resistance $R_s^e = 0.1, 0.4, 1.4, 5.0\,\Omega\,\mathrm{cm}^2$, (c) effective densities of states $N_{T0} = 1 \times 10^{19}, 5 \times 10^{19}, 2 \times 10^{20}, 1 \times 10^{21}\,\mathrm{cm}^{-3}$, and (d) charge carrier mobilities for electrons $\mu_e = 1, 6, 10, 15\,\mathrm{cm}^2\,\mathrm{V}^{-1}\,\mathrm{s}^{-1}$ and holes $\mu_h = 1/3\,\mu_e$. As baseline parameters serve the following values: $E_\mu = 1.75\,\mathrm{eV}$, $R_s^e = 0.4\,\Omega\,\mathrm{cm}^2$, $N_{T0} = 2 \times 10^{20}\,\mathrm{cm}^{-3}$, and $\mu_e = 10\,\mathrm{cm}^2\,\mathrm{V}^{-1}\,\mathrm{s}^{-1}$.

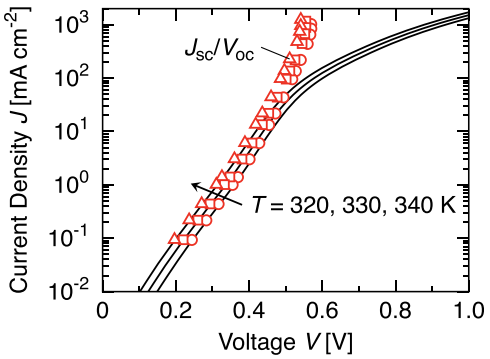

FIG. 6. Experimental dark *JV* characteristics (black solid lines) of μc-Si:H *pin*-type solar cell, and corresponding pairs of short circuit current densities (J_{sc}) and open circuit voltages (V_{oc}) (red open symbols) measured at temperatures $T = 320$, 330, and 340 K.

of parameter values relevant for μc-Si:H and a-Si:H solar cells.

B. Experiment

For the experimental work, we use a μc-Si:H *pin*-type solar cell, deposited with plasma-enhanced chemical vapour deposition (PECVD) from silane and hydrogen at 185 °C.[33–35] The device consists of a highly conductive zinc oxide front contact, a *p*-doped and an intrinsic μc-Si:H absorber layer, and an a-Si:H *n*-doped layer. The back contact consists of a Ag/Al layer stack. In order to avoid current spreading (see Ref. 31), we etch back the silicon layer stack around the contacts. The aluminium protects the underlying silver from the reactive ion etching process.

Under *AM*1.5*G* conditions the solar cell yields an open circuit voltage $V_{oc} = 507\,\text{mV}$ and a short circuit current density $J_{sc} = 16.9\,\text{mA cm}^{-2}$. The fill factor, which is very sensitive to the series resistance, is $FF = 72\%$. These photovoltaic parameters yield a cell efficiency $\eta = 7.2\%$.

The Fig. 6 shows experimental *JV* characteristics, where the temperature $T = 320$, 330, and 340 K is varied. The J_{sc}/V_{oc} pairs at highest V_{oc} show a slight shift to lower voltage, which is probably caused by temperature increasing under high illumination (up to hundred suns).

The Fig. 7 shows R_s and a fit with Eq. (15) to determine $R_s^e = 0.55\,\Omega\,\text{cm}^2$, $E_\mu = 1.20\,\text{eV}$, $N_{T0} = 4 \times 10^{19}\,\text{cm}^{-3}$, and

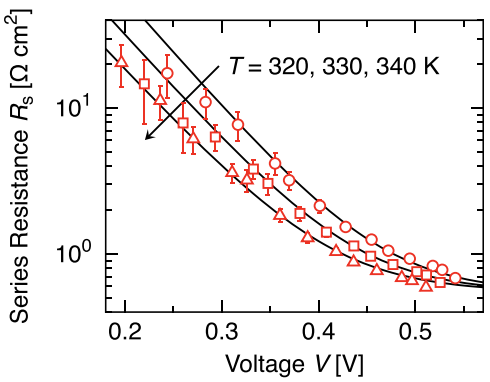

FIG. 7. Fit (black solid lines) of the series resistance after Eq. (6) to the measurements (red open symbols) of a μc-Si:H *pin*-type solar cell with the analytical approximation according to Eq. (15). The temperature is varied in the range $T = 320$, 330, and 340 K.

$\mu_e = 36\,\text{cm}^2\,\text{V}^{-1}\,\text{s}^{-1}$ and $\mu_h = 12\,\text{cm}^2\,\text{V}^{-1}\,\text{s}^{-1}$ for a corresponding reference temperature $T_0 = 300\,\text{K}$. These parameters are in good agreement with previous results.[15,31] Note, however, that this is not a unique fit. From fitting Eq. (15) to measurements, we can unambiguously determine the external series resistance (R_s^e). The value for the mobility gap we used, follows from the temperature dependent dark current density measurements and is therefore also well determined.[15] This way we determine the parallel minimum metallic conductivity to be $qN_{T0}\,(1/\mu_h + 1/\mu_e)^{-1} \approx 58\ \text{S cm}^{-1}$.

V. CONCLUSIONS

The present paper derives an analytical model for the total series resistance (R_s) of low-mobility *pin*-type solar cells as obtained by the J_{sc}/V_{oc} method. Our model allows us to separate the voltage dependent internal resistance of the intrinsic layer from the residual, external resistance. We verified our model over a wide range of parameters relevant to thin-film silicon devices by comparison to numerical simulations. Fitting experimental data obtained from a μc-Si:H *pin*-type solar cell to our model, unveiled an external series resistance of $R_s^e = 0.55\,\Omega\,\text{cm}^2$ and the parallel minimum metallic conductivity of the intrinsic layer of $58\,\text{S cm}^{-1}$, a value that is consistent with a more detailed analysis of similar devices.[15]

[1]P. P. Altermatt, G. Heiser, A. G. Aberle, A. Wang, J. Zhao, S. J. Robinson, S. Bowden, and M. A. Green, Prog. Photovoltaics **4**, 399 (1996).
[2]C. Ulzhöfer, P. P. Altermatt, N.-P. Harder, and R. Brendel, J. Appl. Phys. **107**, 104509 (2010).
[3]S. Steingrube, H. Wagner, H. Hannebauer, S. Gatz, R. Chen, S. Dunham, T. Dullweber, P. P. Altermatt, and R. Brendel, Energy Procedia **8**, 263 (2011).
[4]W. Tress, K. Leo, and M. Riede, Phys. Rev. B **85**, 155201 (2012).
[5]K. Bothe, P. Pohl, J. Schmidt, T. Weber, P. Altermatt, B. Fischer, and R. Brendel, in *21st European Photovoltaic Solar Energy Conference, Dresden* (London: James & James Publisher Ltd., 2006), pp. 1–4.
[6]D. Hinken, K. Ramspeck, K. Bothe, B. Fischer, and R. Brendel, Appl. Phys. Lett. **91**, 182104 (2007).
[7]K. Ramspeck, K. Bothe, D. Hinken, B. Fischer, J. Schmidt, and R. Brendel, Appl. Phys. Lett. **90**, 153502 (2007).
[8]T. Trupke, E. Pink, R. A. Bardos, and M. D. Abbott, Appl. Phys. Lett. **90**, 93506 (2007).
[9]K. Bothe, K. Ramspeck, D. Hinken, and R. Brendel, ECS Trans. **16**, 63 (2008).
[10]R. Brüggemann, Philos. Mag. **89**, 2519 (2009).
[11]R. Brüggemann, Phys. Status Solidi C **9**, 1496 (2012).
[12]O. Breitenstein, J. P. Rakotoniaina, A. S. H. van der Heide, and J. Carstensen, Prog. Photovoltaics **13**, 645 (2005).
[13]J. Isenberg, A. S. H. van der Heide, and W. Warta, Prog. Photovoltaics **13**, 697 (2005).
[14]M. Wolf and H. Rauschenbach, Adv. Energy Convers. **3**, 455 (1963).
[15]B. E. Pieters, H. Stiebig, M. Zeman, and R. A. C. M. M. van Swaaij, J. Appl. Phys. **105**, 044502 (2009).
[16]S. M. Sze and K. K. Ng, *Physics of Semiconductor Devices* (Wiley-Interscience, 2006), Vol. 3.
[17]N. F. Mott, Philos. Mag. **26**, 1015 (1972).
[18]A. R. Moore, Appl. Phys. Lett. **31**, 762 (1977).
[19]W. Fuhs, M. Milleville, and J. Stuke, Phys. Status Solidi B **89**, 495 (1978).
[20]T. Tiedje, C. R. Wronski, B. Abeles, and M. Cebulka, Sol. Cells **2**, 301 (1980).
[21]R. A. Street, J. Kakalios, and M. Hack, Phys. Rev. B **38**, 5603 (1988).
[22]E. A. Schiff, J. Phys.: Condens. Matter **16**, S5265 (2004).
[23]T. Dylla, F. Finger, and E. A. Schiff, Appl. Phys. Lett. **87**, 032103 (2005).
[24]T. Dylla, S. Reynolds, R. Carius, and F. Finger, J. Non-Cryst. Solids **352**, 1093 (2006).

[25]M. Burgelman, J. Verschraegen, S. Degrave, and P. Nollet, Prog. Photovoltaics **12**, 143 (2004).
[26]B. E. Pieters, J. Krc, and M. Zeman, in *Photovoltaic Energy Conversion, Conference Record of the 2006 IEEE 4th World Conference* (IEEE, Piscataway, NJ, 2006), Vol. 2, pp. 1513–1516.
[27]K. Ding, T. Kirchartz, B. E. Pieters, C. Ulbrich, A. M. Ermes, S. Schicho, A. Lambertz, R. Carius, and U. Rau, Sol. Energy Mater. Sol. Cells **95**, 3318 (2011).
[28]T. C. M. Müller, B. E. Pieters, T. Kirchartz, R. Carius, and U. Rau, Phys. Status Solidi C **9**, 1963 (2012).
[29]G. Tao, "Optical modeling and characterization of hydrogenated amorphous silicon solar cells," Ph.D. dissertation (Delft University of Technology, 1994).
[30]M. Zeman, R. A. C. M. M. van Swaaij, J. W. Metselaar, and R. E. I. Schropp, J. Appl. Phys. **88**, 6436 (2000).
[31]J. A. Willemen, "Modelling of amorphous silicon single- and multi-junction solar cells," Ph.D. dissertation (Technische Universiteit Delft, Delft, 1998).
[32]J. Liang, E. A. Schiff, S. Guha, B. Yan, and J. Yang, Appl. Phys. Lett. **88**, 063512 (2006).
[33]O. Vetterl, F. Finger, R. Carius, P. Hapke, L. Houben, O. Kluth, A. Lambertz, A. Mück, B. Rech, and H. Wagner, Sol. Energy Mater. Sol. Cells **62**, 97 (2000).
[34]S. Klein, T. Repmann, and T. Brammer, Sol. Energy **77**, 893 (2004).
[35]B. Rech, T. Roschek, T. Repmann, J. Müller, R. Schmitz, and W. Appenzeller, Thin Solid Films **427**, 157 (2003).